On the accuracy of some mapping techniques used to study the magnetic field dynamics in tokamaks

D Constantinescu[1], O Dumbrajs[2,3], V Igochine[4], B Weyssow[5]

[1]*Department of Applied Mathematics, University of Craiova, A.I.Cuza Street 13, Craiova 1100, (200585) Romania, Association Euratom-Mec Romania*
[2]*Helsinki University of Technology, Association Euratom-Tekes, P.O.Box 2200, FIN-02015 HUT, Finland*
[3]*Institute of Solid State Physics, Association Euratom-University of Latvia, Kengaraga Street 8, LV-1063, Riga, Latvia*
[4]*MPI für Plasmaphysik, Euratom-Association, D-85748 Garching, Germany*
[5] *Statistical and Plasma Physics, Université Libre de Bruxelles, CP 231, Boulevard du Triomphe, 1050 Bruxelles, Belgium, Euratom-Belgian State Association for Fusion*

Abstract: The dynamics of magnetic field lines and of charged particles in toroidal chambers are commonly analyzed by solving numerically the dynamical equations. They may also be analyzed using deterministic reduced models i.e. low dimensional discrete time approximations (maps) of the Hamiltonian continuous time models. We report on the accuracy of the latter method, by considering the mapping technique derived from Hamilton-Jacobi equation. The optimum time stepping in some models for the study of magnetic field in tokamaks is determined by using local criteria. A special attention is given to the analysis of the stochasticity produced by the time discretization.

Keywords: magnetic field in tokamaks, mapping technique
Subject classification numbers (PACS): 52.25.Gj 05.45.Gg, 05.45.Pq

1. Introduction

In tokamaks the charged particles are confined by a magnetic field obtained by the superposition of two basic components acting in the direction of the major, respectively minor curvatures of the torus. It is well known that the magnetic field lines can be regarded as trajectories of a Hamiltonian system obtained from the equations of the magnetic field by using the Clebsh representation [1]. The Hamiltonian of the system is the poloidal magnetic flux and the symplecticity of the Hamiltonian system is the geometrical expression of the magnetic flux conservation property contained in the equations of the magnetic field

The initial equations and the Hamiltonian system describe the three-dimensional configuration of the magnetic field. Because sometimes it is difficult to understand and to interpret complex three-dimensional structures a two-dimensional visualization is useful. The reduction of one dimension can be obtained using the Poincaré map: instead of studying the motion of the magnetic line around the torus, the successive intersections of the magnetic field line with the fixed poloidal section will be considered in order to describe its dynamics

The first application of a Hamiltonian map to the study of the magnetic field in a tokamak (in presence of a magnetic limiter) appears to be due to Martin and Taylor in 1984 [2]. From that moment a lot of mapping models were proposed for the study of various magnetic configurations (only some “hystorical” papers are mentioned here): in 1987 a global model for a specific stellarator (W VII-A) was introduced by Wobig [3], some models of the edge region (scrape-off layer) of a tokamak were studied by Punjabi and co-workers [4] by means of a simple algebraic map and by Abdullaev and Zaslavski [5] using the “separatrix map”, a model compatible with the toroidal geometry was proposed by Balescu [6], some reversed shear magnetic configurations were studied by Davidson and co-workers [7], Oda and Caldas [8], Balescu [9] etc.

For an accurate description of the magnetic field the mapping model must be closely related with the Hamiltonian system. It can be obtained in two philosophically different ways: by numerical integration (using appropriate methods, namely symplectic integrators) with small steps or by the mapping technique that uses large steps. The later is a modern technique providing important advantages: the computational time needed to obtain the phase portrait is several order smaller than for the numerical integration and (which is more important) it has better accuracy in the study of chaotic dynamics, due to the fact that the accumulation of round-off errors is reduced.

Rigorous methods for obtaining discrete models were presented in [10] and [11]. The recent and excellent monograph [12] is a systematic study of the mapping techniques and of their applications.

The mapping technique we focus on in this paper, derived from the Hamilton-Jacobi method, was proposed in [10] by S S Abdullaev. In the paper the author realized also an analysis of the accuracy of the symmetric map by comparing the results obtained using this map with those obtained by the symplectic integration using numerical methods (fifth Runge-Kutta method that was developed by Mc Lachan and Atela). From the analyzed examples it was found that the maps with the time step comparable with the perturbation period have the same accuracy as the symplectic integrators with the integration step two or three orders smaller, hence it represents a powerful tool for the discretization of the Hamiltonian system.

It is obvious that by choosing smaller steps in the symmetric map one obtains results closer to the continuous case, but we are interested in optimizing the computational time, hence an important problem is to choose the largest mapping step for which the main properties of the continuous system are preserved.

The aim of our study is to provide and to use criteria for choosing the largest mapping step for which the symmetric map preserves the main properties of the system.

The paper is organized as follows: in section 2 some basic considerations on the Hamiltonian description of the magnetic field lines and on the mapping technique based on Hamilton-Jacobi method are presented; section 3 is devoted to the criteria we will use for measuring the accuracy of a map; these criteria will be applied in section 4 for determining the optimal mapping step in two models used for the description of the magnetic field in tokamaks; a summary and conclusions are given in section 5.

2 **Basic results**

Because the tokamaks are toroidal devices it is natural to use the toroidal coordinates (r,θ,ζ) in order to describe the configuration of the magnetic field (ζ is the toroidal angle and (r,θ) are the polar coordinates in a circular poloidal cross-section having the radius a), due to the specific form of the device.

The magnetic field $\vec{B}$ with the toroidal flux $\psi=\psi(r,\theta,\zeta)$ is constrained to obey to the conditions

$$\nabla\cdot\vec{B}=0 \qquad \vec{B}\cdot\nabla\psi=0 \tag{1}$$

From the Clebsh representation ($\vec{B}=\nabla\psi\times\nabla\theta+\nabla\zeta\times\nabla H$) is obtained the Hamiltonian system

$$\frac{d\psi}{d\zeta}=-\frac{\partial H}{\partial\theta}, \qquad \frac{d\theta}{d\zeta}=\frac{\partial H}{\partial\psi} \tag{2}$$

which describes the magnetic field configuration. For a circular plasma section the toroidal flux ψ is related to the poloidal radius by $\psi=r^2/(2a^2)$. In this formalism (ψ,θ) appear as a pair of canonical variables. The Hamiltonian of the system is the poloidal magnetic flux $H=H(\psi,\theta,\zeta)=H_0(\psi)+H_1(\psi,\theta,\zeta)$ which can be expressed as a sum of the unperturbed flux $H_0(\psi)=\int\frac{d\psi}{q(\psi)}$ (here $q=q(\psi)$ is the safety factor) and of the perturbation

$$H_1(\psi,\theta,\zeta)=\sum_{m,n}H_{mn}(\psi)\cos(m\vartheta-n\zeta+\chi_{mn}) \tag{3}$$

The variable ζ is interpreted in analogy with a “time” variable, so that the Hamiltonian equations for the magnetic field lines are interpreted as “equations of motion”. In this description of the magnetic field’s configuration we mainly observe the dynamics of the magnetic field lines, for simplicity, in spite of the fact that a magnetic field line remains static and it is just followed along the toroidal direction.

The system (2) is generically non-integrable, so it can be studied only by appropriate numerical methods or by using the Poincare map associated to a transverse cross-section. In modelling phenomena related to the tokamak physics it is natural to use the Poincare map because the poloidal section $(S):\zeta=\zeta_0=cst$ is an ideal Poincare section.

The Poincare map, (also called the first return map) $T:(S)\to(S)$, $T(\psi,\theta)=(\overline{\psi},\overline{\theta})$ is obtained by considering $(\overline{\psi},\overline{\theta},\zeta_0)$ the re-intersection of the magnetic field line starting from (ψ,θ,ζ_0) with (S) after a toroidal turn. In this notation ζ_0 is omitted, because it is a constant. The orbit of the point (ψ_0,θ_0) is $O(\psi_0,\theta_0)=\{(\psi_0,\theta_0),(\psi_1,\theta_1),...,(\psi_n,\theta_n),...\}$, where $(\psi_{k+1},\theta_{k+1})=T(\psi_k,\theta_k)$ for all $k\in N$.

The Poincare map describing the magnetic field lines in tokamaks must have two (independent) properties [1]: to be an area-preserving map (property imposed by the symplecticity of the Hamiltonian system) and to be compatible with the toroidal geometry (i.e. $\psi=0\Rightarrow\overline{\psi}=0$ -which means that the polar axis of the torus is invariant- and $\psi>0\Rightarrow\overline{\psi}>0$ -due to the fact that the toroidal flux $\psi=r^2/(2a^2)$ has only positive values).

In order to obtain a map which is a good approximation of the Poincare map the Hamilton-Jacobi method provides a powerful tool [10]. The first order symmetric map derived in [10] on the basis of the Hamilton-Jacobi method is written as follows:

$$T_N:\begin{cases}\Psi_k=\psi_k-\dfrac{\partial S^{(k)}}{\partial\theta_k} & \Theta_k=\left(\theta_k+\dfrac{\partial S^{(k)}}{\partial\Psi_k}\right)\bmod(2\pi)\\ \overline{\Theta}_k=\left(\Theta_k+w(\Psi_k)(\zeta_{k+1}-\zeta_k)\right)\bmod(2\pi) & \Psi_{k+1}=\Psi_k\\ \theta_{k+1}=\left(\overline{\Theta}_k-\dfrac{\partial S^{(k+1)}}{\partial\Psi_{k+1}}\right)\bmod(2\pi) & \psi_{k+1}=\Psi_{k+1}+\dfrac{\partial S^{(k+1)}}{\partial\theta_{k+1}}\end{cases} \tag{4}$$

where $w(\psi)=1/q(\psi)$ is the spatial frequency of the unperturbed motion and $S^{(k)}=S(\theta_k,\Psi_k)$ is the value of the generating function $G(\theta,\Psi,\zeta,\zeta_0)$ taken at section $\zeta=\zeta_k$, i.e. $S(\theta_k,\Psi_k)=G(\theta_k,\Psi_k,\varphi_k,\varphi_0)$. The first order generating function in the finite interval $\varphi_k\le\varphi<\varphi_{k+1}$ is given by the expression

$$G(\theta,\Psi,\zeta,\zeta_0)=-(\zeta-\zeta_0)\sum_{mn}H_{mn}(\Psi)\times\left[a(x_{mn})\sin(m\theta-n\zeta+\chi_{mn})+b(x_{mn})\cos(m\theta-n\zeta+\chi_{mn})\right]$$

Where $a(x)=[1-\cos(x)]/x$, $b(x)=\sin(x)/x$, $x_{mn}=(m/q(\Psi)-n)(\zeta-\zeta_0)$ and χ_{mn} are phases. For the symmetric mapping the free parameter ζ_0 is taken exactly in the middle of the interval $[\zeta_k,\zeta_{k+1}]$. The sections $\zeta=\zeta_k$ are equally distanced and the mapping step is $\dfrac{2\pi}{N}=\zeta_{k+1}-\zeta_k$ .The first return map is in this case

$$T=\underbrace{T_N\circ T_N\circ\ldots\circ T_N}_{N\ times} \tag{5}$$

In the poloidal section $\zeta=0$ the map T obeys to the condition $T(\psi,2\pi-\theta)=T(\psi,\theta)$ for all $\psi>0$ and $\theta\in[0,2\pi)$ its graph is symmetric to the lines $\theta=\pi$ and $\theta=0$. As a consequence the orbit of any point (ψ,θ) is symmetric to the same lines. In other poloidal sections the orbits are obtained by a rotation of the orbit obtained in the section $\zeta=0$.

A hyperbolic point of any odd periodic orbit is situated on the line $\theta=\pi$ and an elliptic one is situated on the line $\theta=0$. For the periodic orbits with even period an elliptic point is found on the line $\theta=\pi$ and a hyperbolic one is found on the line $\theta=0$. For this reason we will focus our analysis on the dynamics of the map on these lines

3 Criteria for measuring the accuracy of a mapping model

In what follows we will not compare the results obtained using the map (5) with those obtained by using the numerical integration because this analysis was already performed in [10] on various examples. We will compare the accuracy of the map (5) obtained for various N and we propose some criteria for choosing the optimal mapping step.

The strategy is the following: an indicator of the accuracy $IA(N)$ and an acceptable error E are considered and the optimal step N_0 is the smallest N for which $|IA(N+1)-IA(N)|<E$.

In order to compute $IA(N)$ we will consider p equally distanced points situated on the line $\theta=\pi$, a local indicator of the accuracy ($IA_s(N)$, $s=\overline{1,p}$) will be computed and $IA(N)$ will be the average of these values, i.e. $IA(N)=\dfrac{1}{p}\sum_{s=1}^{p}IA_s(N)$.

The local indicator of the accuracy can be chosen by using the following criteria (or maybe others).

Criterion I (The mean energy error criterion)

For the orbit of n points starting from (ψ_0,θ_0) a local indicator of the accuracy is the mean energy error

$$MER(\psi_0,\theta_0)=\left\|H-H(\psi_0,\theta_0)\right\|_2^{\ 2}=\frac{1}{n}\sum_{k=1}^{n}\left(H(\psi_k,\theta_k)-H(\psi_0,\theta_0)\right)^2 \tag{6}$$

This criterion uses the invariance of the Hamiltonian along the orbit and measures the deviation of the Hamiltonian on the mapped orbit from its initial value: in order to describe the local accuracy of the map we check how small the value of $MER(\psi_0,\theta_0)$ is. More accurate mapped orbit corresponds to a smaller value of $MER(\psi_0,\theta_0)$.

Due to the fact that the Hamiltonian is invariant along the orbit only if does not explicitly depend on time (i.e. ζ in our case), this criterion may applied only in a restrained number of cases (example 1 in section 4). However it can be useful also in cases when the Hamiltonian has small variation along the orbits, i.e. $\left|\frac{dH}{d\zeta}\right| = \left|\frac{\partial H}{\partial \zeta}\right| << 1$,(as in the examples studied in section 4). It can be applied for the system with large variation only in the regions closed to elliptic periodic points (inside the magnetic islands) where, due to its continuity and the specific form of the orbits, the Hamiltonian has small variations.

It is maybe useful to remark that the symplectic integrators and the mapping based on the generating function do not always conserve the Hamiltonian along the orbit (even if it is a first integral of the system). Interesting results and comments on this topic can be found in [13] where Chapter IV is devoted to the integration methods that conserve the first integrals and the symplectic integration of Hamiltonian System (including the generating function method) is presented in Chapter VI.

Another way to study the local accuracy of a map is to integrate the system starting from (ψ_0,θ_0) forward in time until a certain "time" instant n, then to integrate the system starting from (ψ_n,θ_n) backward and to check how closed the forward orbit of (ψ_0,θ_0) and the backward orbit of (ψ_n,θ_n) are.

More precisely: The forward orbit of $(\psi_0,\theta_0)$is $O(\psi_0,\theta_0)=\{(\psi_0,\theta_0)....(\psi_n,\theta_n)\}$ and the backward orbit of (ψ_n,θ_n) will be denoted by $O_{inv}(\psi_n,\theta_n.)=\{(\psi'_n,\theta'_n),(\psi'_{n-1},\theta'_{n-1})....(\psi'_0,\theta'_0)\}$

In order to compute the distance between $O(\psi_0,\theta_0)$ and $O_{inv}(\psi_n,\theta_n)$ the distance between the points $A_k(\psi_k\cdot\cos(\theta_k),\psi_k\cdot\sin(\theta_k))$ and $B_k(\psi'_{n-k}\cdot\cos(\theta'_{n-k}),\psi'_{n-k}\cdot\sin(\theta'_{n-k}))$ will be used.

In this case $dist(k)=\sqrt{(\psi_k\cos(\theta_k)-\psi'_{n-k}\cos(\theta'_k))^2+(\psi_k\sin(\theta_k)-\psi'_{n-k}\sin(\theta'_k))^2}$ will represent the error at the k iteration.

Criterion II (The forward-backward error)

For the orbit of n points starting from (ψ_0,θ_0) a local indicator of the accuracy is the forward-backward error

$$FB(\psi_0,\theta_0)=\frac{1}{n+1}\sum_{k=0}^{n} dist(k) \qquad (7)$$

Theoretically speaking the points A_k and B_{n-k} must coincide because they are obtained by using a map and its inverse, but the accumulation of the round-off errors automatically generated by the computer leads to a different situation: when the point (ψ,θ) is mapped one time forward and then one time backward a new point (ψ',θ'), closed to the initial one, will be obtained. Smaller distance between (ψ,θ) and (ψ',θ') is a sign of a better accuracy of the method. It is not always true that by decreasing the mapping step we obtain a better accuracy. It happens in zones with regular dynamics (for librational orbits situated inside the magnetic island or for rotational orbits) but in the chaotic zones, governed by the sensitive dependence on initial conditions, decreasing the mapping step means increasing the accumulations of the round-off errors (because at each step one has to solve complicate implicit equations) and this phenomenon can drastically distort the orbit.

From the previous considerations it results that one can use the forward-backward indicator in order to decide if an orbit is regular or chaotic: a small value of $FB(\psi_0,\theta_0)$(less than 10^{-6} for example) shows that the orbit is regular and a large value of $FB(\psi_0,\theta_0)$ (of order 10^{-1} for example) means that the orbit is chaotic.

Another property of some orbits of the Hamiltonian system that must be preserved by the mapping technique is the rotation number.

The rotation number of the orbit starting from (ψ_0, θ_0) is $RN(\psi_0, \theta_0) = \lim_{k\to\infty} \frac{\theta_k^{\,L}}{2\pi \cdot k}$, where $\theta_k^{\,L}$ is the lift of θ_k (i.e. Θ_k $\overline{\Theta_k}$ and θ_{k+1} are considered without $\mathrm{mod}(2\pi)$ in (4) and (5)), provided that the limit exists. The rotation number of the librational orbits (regular orbits surrounding an elliptic periodic point of type (m,n) is n/m, the rotational orbits have irrational rotation number that can be approximated using a sequence of convergents and it is widely assumed that the chaotic orbits have not rotation number. It is difficult to obtain $RN(\psi_0, \theta_0)$ from its definition due to the weak convergence of the sequence $\left(\theta_k^{\,L}/(2\pi \cdot k)\right)_{k\in N}$, but there are some sophisticated techniques for its accurate computation [14].

Criterion III (The rotation number error)

For a quasiperiodic orbit that starts from (ψ_0, θ_0) and surrounds an elliptic periodic point of type (m,n), a local indicator of the accuracy is rotation number error

$$RNE(\psi_0, \theta_0) = \left| RN(\psi_0, \theta_0) - \frac{n}{m} \right| \tag{8}$$

In order to appreciate the accuracy of the map we check how small is the value of $RNE(\psi_0, \theta_0)$. More accurate mapped orbit corresponds to a smaller $RNE(\psi_0, \theta_0)$.

4 Applications

Some of the criteria introduced in the previous section will be used to determine the optimal mapping step in three cases: for an integrable system, for system having a weak chaotic regime and for a system with a strong chaotic regime.

In order to obtain the mapping model, the Hamiltonian of the system is introduced in the generating function $G(\theta, \Psi, \zeta, \zeta_0)$, then the formula (4) is applied for obtaining the map T_N for various values of N and finally formula (5) will give the Poincare map that generates the mapping model.

4a An integrable model

The first model we will analyze was inspired by the tokamap model [6].

The Hamiltonian of the system is

$$H(\psi, \theta, \zeta) = \frac{1}{4 \cdot q(0)} \cdot \int (2-\psi) \cdot (\psi^2 - 2\psi + 2) d\psi - \varepsilon \frac{\psi}{\psi + 1} \cos\theta \tag{9}$$

The safety factor $q(\psi) = \frac{4 \cdot q(0)}{(2-\psi) \cdot (\psi^2 - 2\psi + 2)}$ was derived in [15] by assuming that the density and electron temperature profiles in the tokamak are, respectively, $n(r) = n(0) \cdot (1 - r^2)$ and $T_e(r) = T_r(0) \cdot (1 - r^2)^2$. Because q is a monotonous increasing function the symmetric map (5) is a twist map. The global perturbation was considered in [6] in order to ensure the compatibility of the symmetric map with the toroidal geometry. The map obtained from (5) will be called HJ-tokamap

In figures 1 and 2 are presented the orbits of 100 equally distanced points situated on the line $\theta = \pi$. The orbits were obtained from (5) for $N = 1$ (figure1a), $N = 2$ (figure2a), $N = 3$ (figure 2b) and $N = 4$ (figure 2c). In the Hamiltonian we considered $q(0) = 1$ and $\varepsilon = 6/(4\pi^2) \approx 0.152$

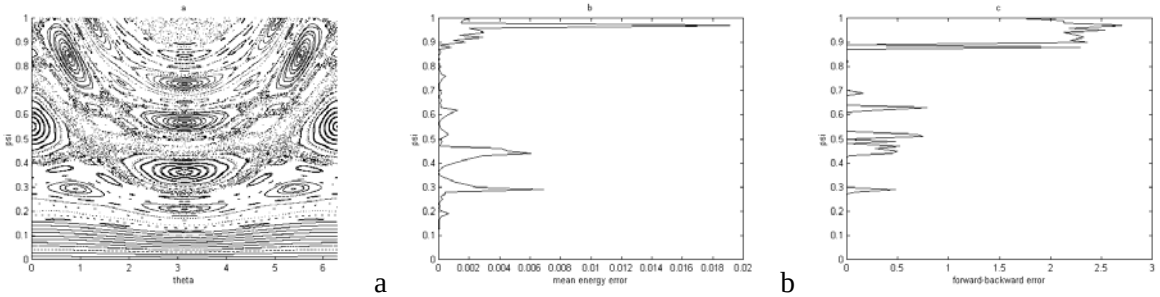

Figure 1 a) the phase portrait of the HJ-tokamap corresponding to $q(0) = 1$ and $\varepsilon = 6/(4\pi^2) \approx 0.152$; b) the mean energy errors of the orbit drawn in fig 1a); The forward-backward errors of the orbits drawn in fig 1a

The Hamiltonian (9) is conserved along the trajectories because it does not explicitly depend on ζ, hence the system is integrable. It means that all the orbits are regular. Due to this specific property, an intuitive determination of the mapping step can be made by analyzing the phase portraits obtained for various N.

In figure 1a, obtained for $N=1$, some large chaotic zones can be observed. It means that the mapping step $2\pi/1$ is too large for a correct description and the stochasticity was artificially introduced. In figure 2a, obtained for $N=2$, the island chains of type $(3,2)$ and $(2,1)$ have a relatively large width, hence thin chaotic layers surround the hyperbolic periodic points, even if they can not be observed in the phase portrait. It means that the mapping step $2\pi/2$ is also too large for a correct description. Due to the fact that the main island chains are very thin in figure 2b (obtained for $N=3$) and practically they can not be observed in figure 2c (obtained for $N=4$) one may consider, intuitively, that the mapping step $2\pi/3$ is convenient but $2\pi/4$ is appropriate for an accurate description of the continuous system. This assertion we will verified by using the criteria presented in section 3.

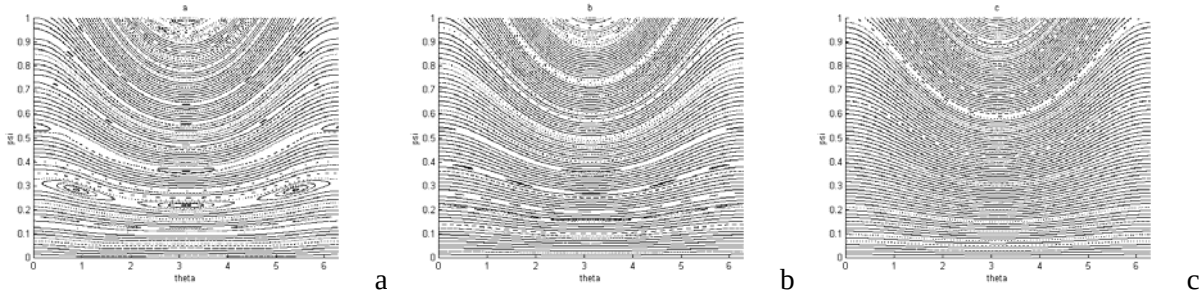

Figure 2 the phase portrait of the HJ-tokamap corresponding to $q(0)=1$ and $\varepsilon=6/(4\pi^2)\approx 0.152$; a) for $N=2$, b) for $N=3$, c) for $N=4$

In order to use Criterion I the mean energy error of each orbit was computed using (6).

In figure 1b are presented the mean energy errors corresponding the orbits presented in figure 1a, obtained for $N=1$. One can observe that local maxima of the mean energy errors correspond to "artificial" chaotic orbits: the chaotic layer surrounding the island chains of type $(3,2)$, $(5,3)$, $(2,1)$ and the chaotic orbits with a large radial motion, i.e. for $\psi > 0.89$.

The global mean energy errors, $MER(N)$, presented in Table 1 were obtained by averaging the mean energy errors of the orbits previously analyzed.

By using the procedure described in Section 3 one can obtain the following results:

- if the admissible error is considered $E=10^{-4}$ the optimal step is $2\pi/2$, corresponding to $N=2$.
- if the admissible error is considered $E=10^{-6}$ the optimal step is $2\pi/3$, corresponding to $N=3$.
- if the admissible error is considered $E=5\cdot 10^{-7}$ the optimal step is $2\pi/4$, corresponding to $N=4$.

For the error $E=10^{-7}$ the corresponding mapping step is $2\pi/6$, corresponding to $N=6$.

	N=1	N=2	N=3	N=4	N=5
MER(N)	0.0008752035	0.0000201613	0.0000009335	0.0000002022	0.0000000762
FBE(N)	0.3244526530	0.1185836725	0.0128944287	0.0000063199	0.0000039593

Table 1

The forward-backward error criterion can be also useful for the study of the accuracy of a mapping model.

The forward-backward errors of the orbits presented in figure 1a, each containing 1000 points, are drawn in figure 1c. As it was expected from theoretical considerations, the local maxima of forward-backward error are obtained for the (artificially introduced) chaotic orbits. This effect is due to the sensitive dependence on initial condition. Because the chaotic orbits surrounding the island chains of type $(3,2)$, $(5,3)$, $(2,1)$ live in a bounded region these maxima are relatively small, but a large variation can be observed for $\psi > 0.89$, i.e. for the chaotic orbits with a large radial motion.

The forward-backward errors, $FBE(N)$, presented in Table 1 were obtained by averaging the forward-backward errors of the orbits.

The values of $FBE(1)$ and $FBE(2)$ are large due to the unbounded chaotic orbits (see figure 1a and figure 2a). For $N=3$ the number of these orbits is reduced and they practically disappear for $N=4$ and $N=5$, hence the forward-backward errors become very small.

Because $FBE(3)-FBE(4)=0.01288810875539$ and $FBE(4)-FBE(5)=0.00000236055637$ one may consider that an appropriate step for the study of the system is $2\pi/4$, corresponding to an admissible error $E=10^{-5}$.

Finally we observe that the criteria we used are independent and there is not a relation between the admissible errors considered for each criterion.

The system we focused on, an integrable one, is a very simple cases. The study we performed before was done in order to verify that the criteria proposed in Section 3 are realistic. But what happens for non-integrable systems?

The non-integrable systems we will study below are particular case of a mapping model proposed in [16] for the study of the magmetic field lines in ASDEX-Upgrade tokamak

4b A system in a weak chaotic regime

These models are closely related to the experiments realized in ASDEX-Upgrade tokamak, even if the determinations of the safety factor and of the perturbation is a challenging task, because of the large uncertainties in the measurements.

The safety factor, $q(\psi)=0.8+4\psi$, describes correctly the experimental position of the MHD modes in ASDEX Upgrade and the perturbations

$$H_{m,n}=\rho_{m,n}\cdot\begin{cases}\alpha\left(\dfrac{\psi}{\psi_{m,n}}\right)^{m/2}\left[1-\beta\left(\dfrac{\psi}{\psi_{m,n}}\right)^{1/2}\right], & \psi\le\psi_{mn}\\ \dfrac{\alpha(1-\beta)-\gamma+\gamma\left(\dfrac{\psi}{\psi_{mn}}\right)^{1/2}}{\left(\dfrac{\psi}{\psi_{mn}}\right)^{(m+1)/2}}, & \psi>\psi_{mn}\end{cases} \qquad (10)$$

were deduced from ECE measurements.

The Hamiltonian of the system is

$$H(\psi,\theta,\zeta)=H_0(\psi)+H_1(\psi,\theta,\zeta)=\frac{\ln(0.8+4\psi)}{4}+\sum_{m,n}H_{m,n}(\psi)\cdot\cos(m\theta-n\zeta) \qquad (11)$$

It our study we will use $\alpha=0.04,\ \beta=0.87,\ \gamma=0.005$, values derived from experiment

The radial positions of the $(3,2)$, $(4,3)$ and $(1,1)$ NTM in the ideal system are $\psi_{3,2}=0.175$, $\psi_{4,3}=0.133$ and $\psi_{1,1}=0.05$.

Because the $(3,2)$ and $(1,1)$ modes are separated by a quite large distance ($\psi_{3,2}-\psi_{1,1}=0.1745$) they will not overlap for moderates values of the perturbations amplitudes. If they are locked together they will generate a (nonintegrable) system having a weak chaotic regime, in the sense that the chaotic zones surrounding the $(3,2)$ mode, respectively the $(1,1)$ mode are thin layers that do not intersect and the influence of a mode on the dynamics near another mode is small.

In this case the Hamiltonian of the system is

$$H(\psi,\theta,\zeta)=H_0(\psi)+H_1(\psi,\theta,\zeta)=\frac{\ln(0.8+4\psi)}{4}+H_{3,2}(\psi)\cdot\cos(3\theta-2\zeta)+H_{1,1}(\psi)\cdot\cos(\theta-\zeta) \qquad (12)$$

We will call the map generated by the Hamiltonian (12) the WCR-ASDEX map (weak chaotic regime ASDEX map)

We are interested whether these chaotic zones are determined by some intrinsic properties of the system or are they generated by the numerical imperfections of the discrete model (as happened in the previous example for the mapping step 2π.

The amplitudes of the Hamiltonian perturbations are $\rho_{3,2} = 0.0875$ and $\rho_{1,1} = 0.0475$,

The phase portrait presented in figure 1a illustrates the previous considerations. It was obtained from formula (5) for $N = 1$, but similar figures can be obtained for $N = 2$, $N = 3$, $N = 4$. A detail of the phase portrait, the region situated near the $(3,2)$hyperbolic point situated on the line $\theta = \pi$, is presented in figure 3b. The black points are obtained using the mapping model with the step $2\pi/1$, the blue points correspond to the mapping step $2\pi/2$, the green ones were obtained by using the mapping step $2\pi/3$ and the red orbits correspond to $2\pi/4$. It can be observed that the regular orbits practically coincide for all considered values of N and the chaotic layer is not smaller for larger N. From these pictures we intuitively conclude that the weak chaos is a property of the system and that there are not important differences between the mapping models obtained for $N \in \{1,2,3,4\}$

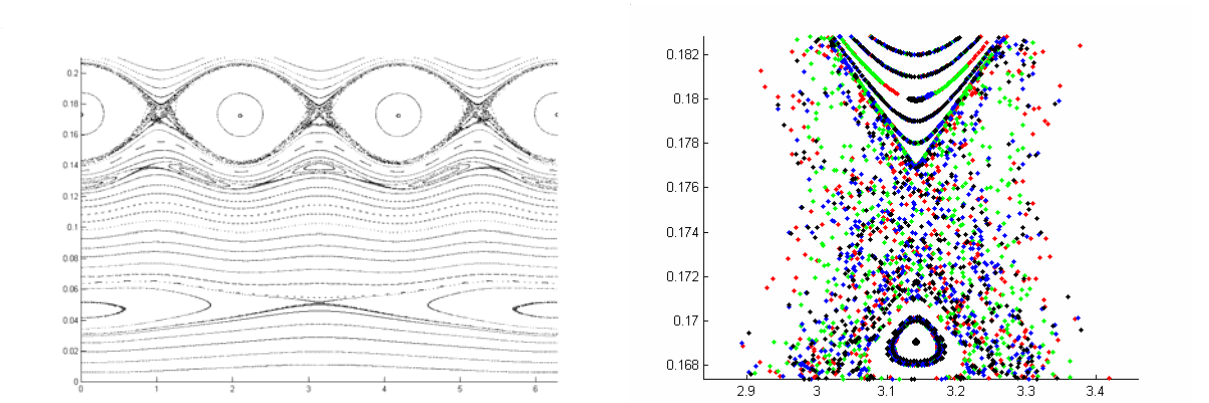

a b

Figure 3 a) Phase portrait of WCR-ASDEX map corresponding to $\alpha = 0.04$, $\beta = 0.87$, $\gamma = 0.005$, $\rho_{3,2} = 0.0875$ and $\rho_{1,1} = 0.0475$, obtained for $N = 1$; b) Detail pf the phase portrait: black points for N=1, blue points for N=2, green points for N=3 and red points for N=4;

For a rigorous study the criteria introduced in section 2. We focus on the annulus $0.12 \le \psi \le 0.24$ because in this region is situated the $(3,2)$ mode. In order to capture the main dynamical properties of the system, 120 orbits starting from equally distanced points on the line $\theta = \pi$ and having 5000 iterations, have been analyzed.

The mean energy errors for these orbits are presented in figure 4a (black points for $N = 1$, blue points for $N = 2$, green points for $N = 3$, respectively red points for $N = 4$. The fact that the orbits corresponding to various N coincide is reflected in the quasi coincidence of the mean energy errors curves.

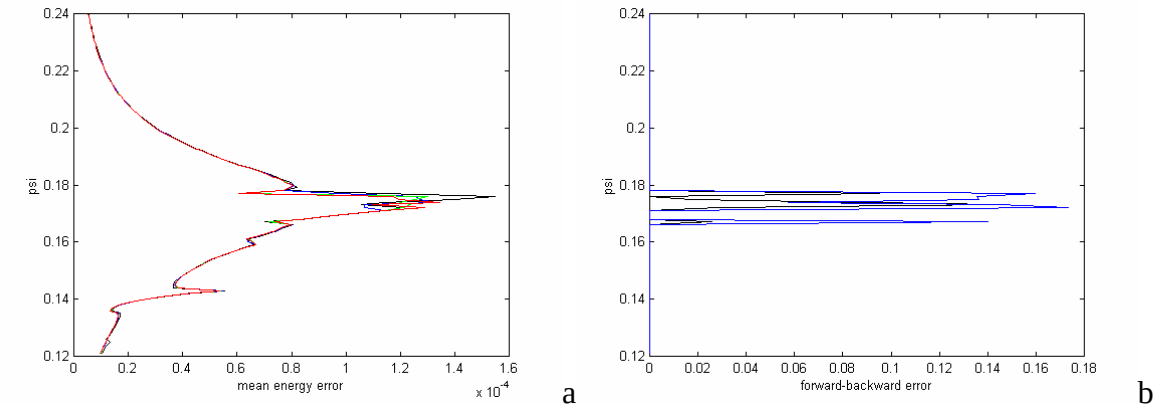

a b

Figure 4 The local mean energy error for WCR-ASDEX corresponding to $\alpha = 0.04,\ \beta = 0.87,\ \gamma = 0.005$, $\rho_{3,2} = 0.0875$ and $\rho_{1,1} = 0.0475$. Black line for N=1, blue line for N=2, green line for N=3 and red line for N=4 ; b) forward-backward error

The largest values of the mean energy error are obtained for $\psi \approx 0.175$, i.e. near the hyperbolic periodic point and they are the sign of the presence of chaos;
The values of the global mean energy errors can be found in Table 2

	N=1	N=2	N=3	N=4
MER(N)	0.0000394194	0.0000387736	0.0000386129	0.0000385294
FBE(N)	0.0033579657	0.0078962707	0.0074237683	0.0073296542

Table 2

Using the method described in section 2 one can find the optimal mapping step for a prescribed admissible error:

- for an admissible error $E = 10^{-5}$ the optimal step is obtained for $N = 1$
- for an admissible error $E = 10^{-6}$ the optimal step is obtained for $N = 2$

In order to use the forward-backward error as an indicator of the accuracy of the mapping model the local forward-backward errors of the 120 orbit considered in the previous study were computed . The results are plotted in figure 4b. One can observe a large peak in the same region where the large values of the mean energy error are situated. It indicates the existence of chaotic orbits, due to the sensitive dependence on initial conditions.
The values of the global forward-backward errors (see Table 2) point out an interesting and unexpected situation: the error corresponding to $N = 2$, i.e. $FBE(2) = 0.0078962707$, is larger than the error obtained for $N = 1$ and values comparable with $FBE(2)$ are obtained for $N = 3$ and $N = 4$.
This means that the chaotic zone surrounding the hyperbolic points is (a little bit) larger in the models obtained for $N \in \{2,3,4\}$ than in the model built by considering $N = 1$. This phenomenon is confirmed by the figure 4b. The explanation can be the following: by modifying the mapping step the orbits situated near the boundary of the chaotic zone are affected because, due to the accumulation of round-off errors, some regular orbits are pushed in the chaotic zone and remain there.
The optimal mapping step is obtained by applying the procedure described in section 2:
-for the admissible error $E = 10^{-2}$ the optimal step is obtained for $N = 1$
- for the admissible error $E = 10^{-3}$ the optimal step is obtained for $N = 2$
- for the admissible error $E = 10^{-4}$ the optimal step is obtained for $N = 3$
In conclusion, in this case the chaotic area is (slightly) enlarged be decreasing the mapping step, then the process is stabilized.

4c A system in a strong chaotic regime

In order to obtain a model in a strong chaotic regime we will consider in the Hamiltonian (11) the perturbations corresponding to the (3,2) and (4,3) NTM. In the unperturbed case these modes are situated on the line $\psi_{3,2} = 0.175$, respectively $\psi_{4,3} = 0.133$. They are relatively closed, hence for moderate amplitudes of the perturbations they will overlap producing a large chaotic zone surrounding both modes. This is the situation we call strong chaotic regime.
The Hamiltonian of the system is

$$H(\psi,\theta,\zeta) = H_0(\psi) + H_1(\psi,\theta,\zeta) = \frac{\ln(0.8+4\psi)}{4} + H_{3,2}(\psi)\cdot\cos(3\theta - 2\zeta) + H_{4,3}(\psi)\cdot\cos(4\theta - 3\zeta). \quad (13)$$

The map obtained from (4) and (5) using the Hamiltonian (12) will be called SCR-ASDEX (strong chaotic regime in ASDEX).
In figure 5a is presented the phase portrait of the map for which only the (3,2) mode was activated, i.e. $\rho_{3,2} = 0.0875$ and $\rho_{4,3} = 0$, obtained from (5) for $N = 1$. The width of the islands surrounding the elliptic points is large due to the quite large value of the amplitude perturbation $\rho_{3,2}$. The (4,3) mode

can be observed in the lower part of the figure. Figure 5b shows the phase portrait of the SCR-ASDEX map when the $(3,2)$ and $(4,3)$ modes are locked together, obtained for $N=1$ (black points), $N=2$ (blue points) and $N=3$ (red points). The amplitudes of the perturbations that we use in the analysis are $\rho_{3,2}=0.0875$ and $\rho_{4,3}=0.0428$. A large chaotic zone surrounding the two modes was formed because they overlap, but it is practically the same for all values of N. In the upper part of the figure 5b one can observe in the phase portrait obtained for $N=1$ (black points) an island chain which is reduced to a rotational orbit in the phase portrait obtained for $N=2$ and $N=3$.

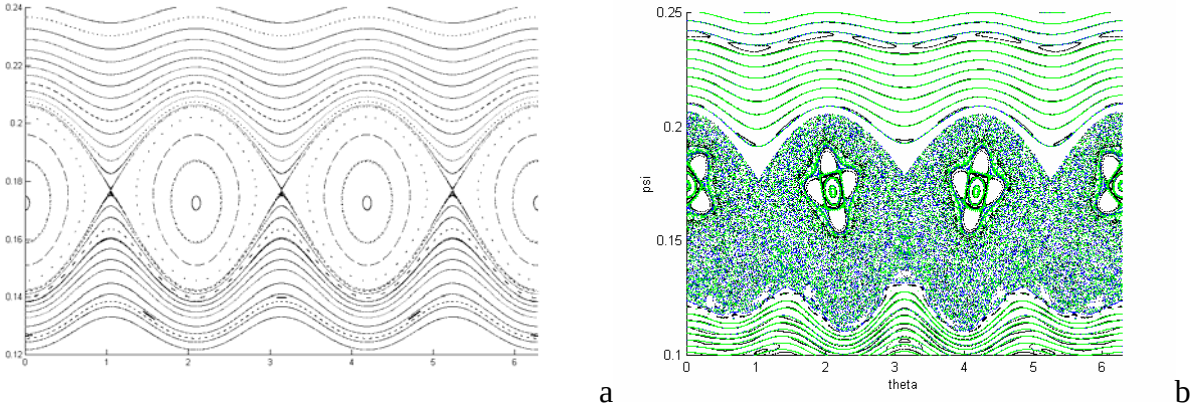

a b

Figure 5. a) Phase portrait of the SCR-ASDEX map, $\rho_{3,2}=0.0875$, $\rho_{4,3}=0$, $N=1$. b) Phase portrait of the SCR-ASDEX map, $\rho_{3,2}=0.0875$, $\rho_{4,3}=0.0428$, $N=1$.

In order to compute the mean energy error 165 orbits starting from points situated on the line $\theta=0$ from $\psi=0$ to $\psi=0.5$ were considered. The local mean energy error of these orbits are plotted in figure 6, for $N=2$, (blue line) and $N=3$ (green line).

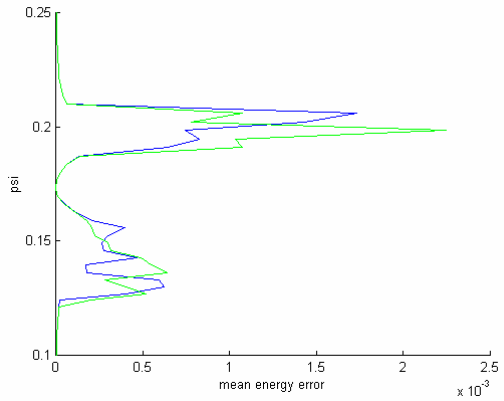

Figure 6 The local mean energy errors for the SCR-ASDEX map, $\rho_{3,2}=0.0875$, $\rho_{4,3}=0.0428$, and $N=2$. (blue line), $N=3$ (green line)

Quite large values of the local mean energy error are observed in the chaotic zone $0.13<\psi<0.18$, which is natural, and near $\psi=0.2$ where the orbits are regular but have a strongly curved shape.
The values of the global mean energy error for are given in table 3.

	$N=1$	$N=2$	$N=3$
MER(N)	0.0000072152	0.00000610545	0.0000068490
FBE(N)	0.0000356473	0.00003275692	0.0000339241

Table 3

For the admissible error $E=10^{-5}$ the optimal step is 2π obtained for $N=1$.
For the admissible error $E=10^{-6}$ the optimal step is π, obtained for $N=2$.
The values of the global forward-backward errors obtained for $N\in\{1,2,3\}$ are very close.

For an admissible error $E = 10^{-5}$ the optimal step is 2π
In this case the mapping model with the step 2π is a sufficiently accurate discretization of the considered Hamiltonian system. This step was used in [16].

5. Conclusions

The work was focused on the study of the accuracy of the mapping models obtained from Hamiltonian systems by using the Hamilton-Jacoby method. Instead of the indicators of numerical accuracy (usually the magnitude of the larger neglected term in an expansion in series) we used some "dynamical" indicators (the mean energy error and the forward-backward error, the rotation number error), specific for this type of models. Three global criteria of accuracy were considered and two of them were used for determining the optimal mapping step in three situations: an integrable model (where the criteria were used only for proving that they are realistic), a system having a weak chaotic regime and a system having a strong chaotic regime.

For a future work one could think about more sophisticated indicators for choosing the optimal step of the mapping in chaotic regimes. For example, the corresponding time series in principal contain two components of chaos: intrinsic and artificial due to insufficient accuracy of the mapping. By analyzing the Fourier spectra of the series obtained for different values of N it should be possible to separate the two components and to draw some conclusions about the optimal step.

Acknowledgements

Helpful discussions with S.S. Abdullaev, R. Balescu and K. Spatschek on various aspects of mappings and their applications are highly acknowledged.

Refererences

[1] Balescu R 1988 *Transport processes in plasmas* Elsevier North-Holland, Amsterdam
[2] Martin T J and Taylor J B 1984 *Plasma Phys. Controlled Fusion* **26** 321
[3] Wobig H 1987 *Z. Naturforsch. Teil* A **42** 1054
[4] Punjabi A, Verma A and Boozer A 1992 *Phys. Rev. Lett* **69** 3392
Punjabi A, Verma A and Boozer A 1994 *J. Plasma Phys.* **52** 1994
Punjabi A, Ali H, Boozer A 1997 *Phys. Plasmas* **4** 337
[5]Abdullaev S S and Zaslavski G M 1995 *Phys Plasmas* **2** 4533
Abdullaev S S and Zaslavski G M 1996 *Phys Plasmas* **3** 516
[6] Balescu R, Vlad M and Spineanu F 1998 *Physical Review* E **58** 951
[7] Davidson M G, Dewar R L, Gardner H. J and Howard J 1995 *Australian Journal of Physics* **48** 871
[8] Oda G A and Caldas I L 1995 *Chaos, Solitons and Fractals* **5** 15
[9] Balescu R 1998 *Physical Review* E **58** 3781
[10] Abdullaev S S 2002 *J. Phys. A, Math. Gen* **35** 2811
[11] Abdullaev S S 2004 *Nuclear Fusion* **44** S12
[12] Abdullaev S S 2006 *Construction of mappings for Hamiltonian systems and their applications* Lect. Notes Phys. 691 Springer Verlag Berlin, Heidelberg New York
[13] Hairer E, Lubich C and Wanner G 2002 *Geometric Numerical Integration, structure-preserving algorithms for ordinary differential equations* Springer Verlag Berlin Heidelberg New York
[14] Efstathiou K and Voglis N 2001 *Physica D* **158** 151
[15] Misguich J H and al 2003 *Annales de Physique* **28** 1-101
[16] Igochine V, Dumbrajs O, Constantinescu D, Zohm Z, Zvejnieks G and ASDEX Upgrade Team 2006 *Nuclear Fusion* **46** 741